THE JOURNAL OF PHYSICAL CHEMISTRY C
A JOURNAL OF THE AMERICAN CHEMICAL SOCIETY

Open Access
This article is licensed under CC-BY 4.0

pubs.acs.org/JPCC
Article

5-Hydroxy-L-tryptophan Adsorbed at the Silver Nanoparticle Surface: Conformational Geometries Revealed by SERS and Multiscale Modeling

Caio Hiroaki Miyake, Jayr Henrique Marin, Gabriel Conishi Cardozo, Diogo Soga, Evandro Luiz Duarte, Antonio Rodrigues da Cunha, Rômulo Augusto Ando, and Erix Alexander Milán-Garcés*

Cite This: J. Phys. Chem. C 2025, 129, 20313−20326

Read Online

ACCESS | Metrics & More | Article Recommendations | Supporting Information

ABSTRACT: 5-Hydroxy-L-tryptophan (5-HTP) is a biologically relevant metabolite and a promising optical probe. However, its vibrational properties have remained poorly characterized. In this work, we present a comprehensive normal Raman and surface-enhanced Raman scattering (SERS) study of 5-HTP by combining experimental results with molecular dynamics (MD) simulations and density functional theory (DFT) calculations. The DFT calculation accurately reproduced the normal Raman spectrum of 5-HTP, which confirmed the zwitterionic nature of the molecule in the solid state. We also report here, for the first time, the SERS spectrum of 5-HTP using silver nanoparticles. The SERS spectrum revealed significant differences in the relative band intensities compared to the normal Raman spectrum, which is related to the adsorption and orientation of the molecule at the metal surface. MD simulations considering neutral and charged silver surfaces showed that 5-HTP does not adopt a unique configuration but interacts primarily through the carboxylate group and often with the indole ring tilted or parallel to the surface. DFT calculations of 5-HTP adsorbed on silver clusters of ten atoms further support these findings and allow us to describe the role of both chemical and electromagnetic effects in the intensity enhancement. This work reported the Raman fingerprint of 5-HTP and its SERS enhancement mechanisms, offering new possibilities for future application of this molecule as a Raman probe in biochemical sensing and protein structure studies.

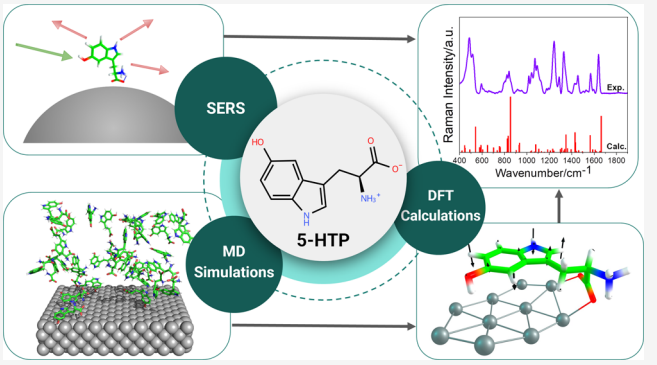

INTRODUCTION

5-Hydroxy-L-tryptophan (5-HTP) is an intermediate in the biosynthesis of the neurotransmitter serotonin (5-HT) formed from the amino acid tryptophan (Trp) via hydroxylation (I) and subsequent decarboxylation (II)[1−4] (Figure 1). The 5-HTP structure is analogous to that of Trp except for the addition of a hydroxyl group to the indole ring. By modulating the serotonin levels in the brain, 5-HTP plays a central role in regulating depression, sleep cycles, and stress.[2,5] 5-HTP also has a significant potential to treat depression,[6−8] migraines, Alzheimer's disease, and Parkinson's disease.[5,9] However, the excessive use of this metabolite can lead to harmful consequences, such as serotonin syndrome, characterized by altered mental conditions and neuromuscular abnormalities. In severe cases, it can cause hyperthermia, multiorgan failures, and cardiac symptoms.[10]

Apart from its biological and medical relevance, 5-HTP has also been used as an extrinsic optical probe of proteins,[4,11] due to its distinct absorption and fluorescence properties compared to Trp.[12] For example, the absorption spectrum of 5-HTP is red-shifted in comparison to that of Trp. Therefore, a single Trp in a multi-Trp protein can be mutated by 5-HTP, and using excitation at 310−320 nm, it is possible to photoexcite 5-HTP without contribution from other aromatic amino acids.[13] Thus, it is possible to selectively probe a specific site in the protein using this approach to obtain information about solvation, structure, and dynamics. For example, Ross et al.[11] inserted 5-HTP in the bacteriophage λcI repressor, a protein that contains three Trp residues. Similarly, Steward et al.[12] studied the site-specific incorporation of 5-HTP as a fluorescent probe of a Trp-rich enzyme, β-Galactosidase. Thus, the use of 5-HTP is especially valuable in the study of proteins containing multiple tryptophan residues, as selective incorporation of 5-HTP allows for simplified spectral interpretation and the investigation of site-specific structure and dynamics of proteins.

Received: September 2, 2025
Revised: October 13, 2025
Accepted: October 22, 2025
Published: October 29, 2025

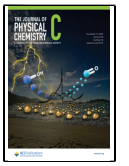

Downloaded via UNIV OF SAO PAULO on December 9, 2025 at 16:17:36 (UTC).
See https://pubs.acs.org/sharingguidelines for options on how to legitimately share published articles.

© 2025 The Authors. Published by American Chemical Society

https://doi.org/10.1021/acs.jpcc.5c06154
J. Phys. Chem. C 2025, 129, 20313−20326

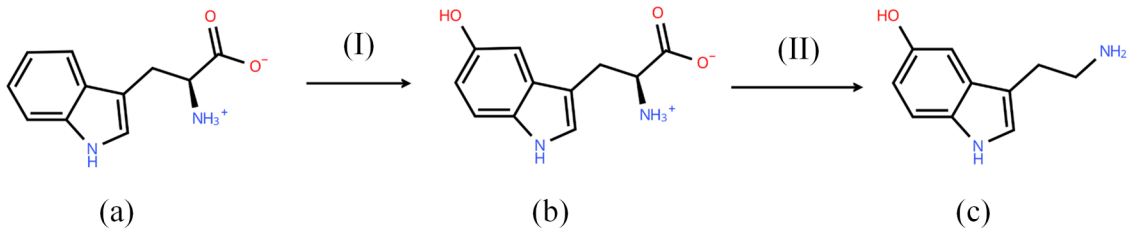

Figure 1. Molecular structures of (a) Trp, (b) 5-HTP, and (c) 5-HT.

Despite these advantages, the use of 5-HTP has been largely limited to fluorescence-based methodologies, and its potential as a Raman active probe has not been explored. Raman spectroscopy offers a complementary approach to fluorescence, providing vibrational fingerprints of molecular structures and enabling the investigation of protein conformations and dynamics at the molecular level without the need for extrinsic labels.[14,15] Particularly, ultraviolet resonance Raman spectroscopy has been used to probe solvation, tertiary contacts, and secondary structure of proteins.[16−18] The Raman signal of Trp and other aromatic amino acids is enhanced by excitation in the 210−230 nm region.[19] Similar to the absorption and fluorescence counterparts, the interpretation of the Raman spectrum of a protein with multiple Trps and aromatic amino acids can be a challenge, as all these residues contribute to the total signal. To solve this, a common approach is to leave a single Trp in the protein by mutating the others with phenylalanine (Phe). For example, in the work of Milán-Garcés et al. of barstar, a protein that contains three Trp residues was mutated into a single Trp-containing form in which a CH−π interaction between the aromatic rings of Trp53 and Phe56 was detected.[20] In another work of Sanchez et al.,[21] the outer membrane protein OmpA had its native Trp residues mutated by Phe in different locations in the protein, enabling it to probe site-specific molecular interactions and protein folding mechanisms.[21]

Over the past two decades, there has been increasing interest in the application of the nano plasmonic variant of Raman spectroscopy, known as surface-enhanced Raman scattering (SERS). SERS enables the study of biological molecules at very low concentrations due to its ability to obtain a significant enhancement in the Raman signal, sufficient for reaching the single-molecule regime.[22−24] SERS has been widely applied to probe biomolecules such as proteins, nucleic acids, amino acids, and neurotransmitters, including Trp and 5-HT.[25−30] In this context, numerous studies have focused on the use of SERS to monitor metabolic alterations, and particular attention has been given to detecting Trp[31−33] and 5-HT.[34−36] These two molecules have been widely characterized by conventional Raman spectroscopy and, more specifically, through SERS. Surprisingly, in the case of 5-HTP, despite its biological relevance and unique optical and chemical properties, it has not been well studied by using Raman techniques.

To our knowledge, the only Raman study of 5-HTP was recently published,[37] reporting the normal Raman spectrum in solid state and its calculated spectrum, which failed to reproduce the experimental results. Therefore, the aim of the present work was to provide a detailed characterization of both the normal Raman and SERS spectra of 5-HTP. The enhancement of the Raman intensities in SERS arises from different mechanisms,[38] including the electromagnetic effect and chemical effect.[39] The contribution of each effect to the signal enhancement can vary considerably depending on the nanoparticle size and morphology, the molecular identity, excitation wavelength, and other local environment factors.[40] As a result, the accurate prediction and assignments of SERS intensities remain a challenge. To address this, the combined use of molecular dynamics (MD) simulations[41,42] and density functional theory (DFT)[43] calculations can provide valuable insights into the molecular conformations and vibrational assignments of 5-HTP relevant to understanding its interaction with SERS substrates. A comprehensive vibrational analysis and SERS response of 5-HTP can provide valuable insights for understanding, for example, its structural changes, solvation, and interactions in biological environments.[44,45] This is particularly essential in protein studies, where selective incorporation of 5-HTP can yield unique spectral markers, and in studies of serotonin-related pathways.[46]

METHODS

Experimental Section. *Materials.* Silver nitrate ($AgNO_3$) (≥98% purity), sodium citrate, and sodium nitrate ($NaNO_3$) were obtained from Merck. Ultrapure water obtained with a Millipore Synergy purification system was employed in the preparation of silver nanoparticles (AgNPs) and all sample solutions.

Synthesis of Nanoparticles. The silver nanoparticles used in this study were synthesized following the Lee−Meisel method,[47] which involves the chemical reduction of silver nitrate by sodium citrate in aqueous solution. For the SERS measurements, the colloidal nanoparticles were centrifuged for 10 min at 6000 rpm to remove the excess of citrate. The supernatant was discarded, and the nanoparticle was redispersed in water maintaining the initial nanoparticle concentration.

Raman Spectroscopy Experiments. The normal Raman spectrum of solid-state 5-HTP was recorded using a Bruker FRS100/s FT-Raman spectrometer with a 1064 nm excitation wavelength, 512 scans, and a laser power of 75 mW. The SERS measurements were carried out in a RENISHAW InVia confocal Raman microscope and were acquired in triplicate with 5 accumulations and 10 s with an excitation wavelength of 785 nm and laser power of 1% (20 mW). For each SERS measurement, a total volume of 200 μL was prepared by sequentially mixing 50 μL of 5-HTP solution with 50 μL of 200 mM $NaNO_3$, followed by the addition of 100 μL of silver colloids. The spectra were subject to baseline correction, and the band positions in the Raman spectra were determined through spectral deconvolution using Lorentzian functions.

Computational Details. *MD Simulations.* The MD simulations were performed following a modified protocol proposed by Roccatano et al.[48] The two models consist of silver surfaces in both neutral and charged states. The latter was constructed by assigning a positive charge to ten atoms

https://doi.org/10.1021/acs.jpcc.5c06154
J. Phys. Chem. C 2025, 129, 20313−20326

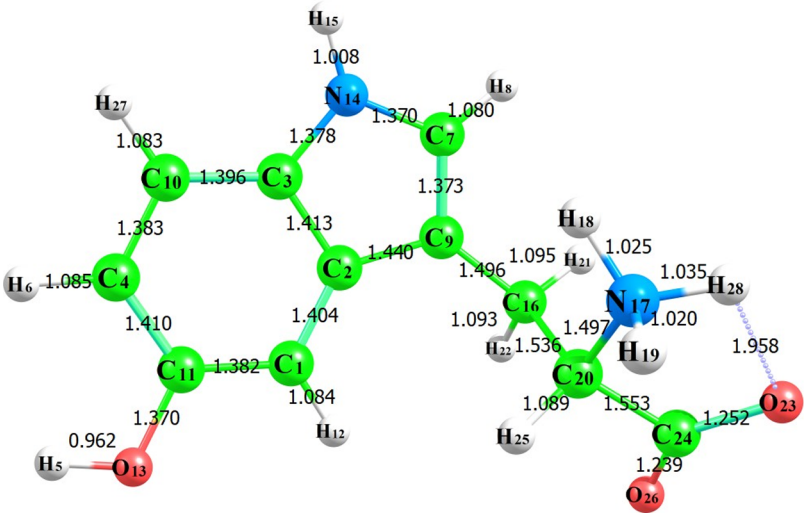

Figure 2. Optimized molecular structure of 5-HTP with atom numbering and bond distances in angstroms (Å) obtained from DFT calculation at the M06-2X/6-311++G(d,p) level and implicit solvation.

uniformly distributed across the surface. The silver surface was positioned at the bottom of the simulation box, and the 5-HTP molecules were initially randomly distributed.[48] The systems were solvated with water molecules. Only the water and 5-HTP molecules were allowed to diffuse freely, while the atoms of the silver surface were restrained at fixed positions. The simulations were performed using the GROMACS 2022[41] Software. The CHARMM36 force field parameter set[49,50] was used for 5-HTP, and the metal atoms and the TIP3P model[51] were used to describe the water molecules. The systems were subject to energy minimization using 10,000 steps of the steepest descent algorithm, followed by 250 ps of equilibration in the NVT ensemble, employing the Berendsen thermostat[52] at 300 K with a coupling constant (tcoupl) of 0.1 ps. The production step was carried out in the NPT ensemble for 200 ns. During this step, the temperature was maintained at 300 K using the Nose−Hoover thermostat[53] with a tcoupl of 1.0 ps, and the pressure was maintained at 1 bar using the Parrinello−Rahman barostat.[54] Semi-isotropic pressure coupling was applied using an isothermal compressibility of 4.6×10^{-5} bar^{-1} and a coupling constant of 1 ps. For all simulations, a cutoff of 1.4 nm was used for short-range nonbonded interactions, while the Particle Mesh Ewald method[55] was employed to compute long-range electrostatic interactions. All bond lengths within the molecules were constrained using the LINCS algorithm.[56] The most representative configurations in which 5-HTP was adsorbed on the silver nanoparticle surface (i.e., the most frequent during the simulation) were selected for quantum mechanics (QM) calculations. To simplify the QM calculations, only a cluster of ten metal atoms near the 5-HTP molecule was explicitly included, while the rest of the silver nanoparticle surface was omitted. The planar silver atom cluster was selected to represent the local environment of the silver nanoparticle surface, which allowed us to describe the interactions of the carboxylate, amino, and indole ring groups of 5-HTP with Ag atoms. Previous studies have shown that small silver clusters reproduce the charge-transfer and vibrational properties of surface-active sites with good accuracy while maintaining computational efficiency.[31,57,58] Similar planar clusters have been successfully applied in SERS studies of amino acids and aromatic molecules such as tryptophan.[31,58] The MD simulations images were obtained using PyMol software.[59]

DFT Calculations. All DFT calculations were performed using the Gaussian 09 Software.[60] The geometries of 5-HTP in its isolated form and adsorbed on the silver cluster, were optimized using the M06-2X functional[61] in combination with a mixed basis set: 6-311++G(d,p) for nonmetallic elements and LANL2DZ for silver atoms.[57,62,63] Solvent effects on the geometries were included using the default polarizable continuum model (PCM)[64] at the same level of theory. The functional M06-2X has been demonstrated to be a very accurate model for noncovalent interactions and organometallics.[61] The vibrational Raman frequencies and activities of all of the optimized structures were calculated at the same level of theory. The assignments of the normal vibrational modes obtained from the DFT calculations were performed by comparing the calculated and experimental spectra, considering both the positions and relative intensities of the bands. The normal mode description was obtained from the output of the Vibrational Energy Distribution Analysis (VEDA) program,[65] complemented by inspection of the atomic motions with the software Chemcraft.[66] The figures containing the optimized molecular structures were obtained by using software Chemcraft.[66]

RESULTS AND DISCUSSION

In this study, we performed geometry optimization and normal mode calculations of 5-HTP in its zwitterionic form[67,68] using DFT methods. The optimized molecular geometry with the atom numbering is shown in Figure 2, and the atomic coordinates are provided in Table S1. The optimized geometry was found to have a planar π-conjugated core and to exhibit an intramolecular hydrogen bond between oxygen O9 and hydrogen H28, in good agreement with the geometries previously obtained using DFT and crystallographic data.[68]

Figure 3 shows the comparison between the calculated and the experimental normal Raman spectrum of solid-state 5-HTP. Although a theoretical spectrum for 5-HTP has been previously reported, it showed limited agreement with experimental data.[37] In contrast, the calculated spectrum obtained in this work demonstrates excellent agreement with

https://doi.org/10.1021/acs.jpcc.5c06154
J. Phys. Chem. C 2025, 129, 20313−20326

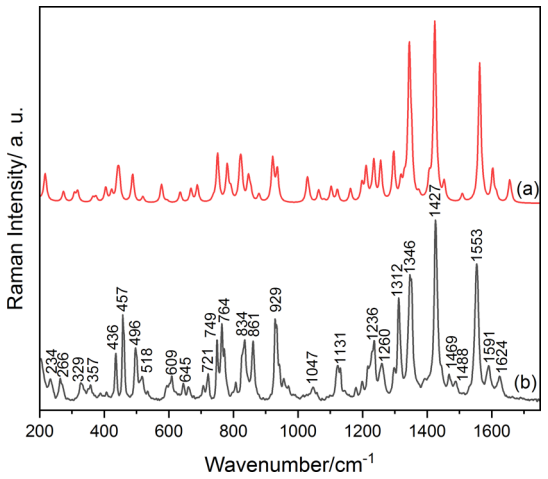

Figure 3. (a) Calculated Raman spectrum of the optimized structure of 5-HTP using a scaling factor of 0.97 and (b) experimental normal FT-Raman spectrum of solid-state 5-HTP recorded with 1064 nm excitation wavelength.

the experimental band positions and relative intensities. Notably, below 1000 cm^{-1}, the computed vibrational frequencies match very well with the experimental bands, while, for higher calculated frequencies, a scaling factor of 0.97 was applied to improve the correlation and to enable more accurate spectral assignment.[69]

A detailed list of both experimental and calculated (scaled and unscaled) band positions, along with the tentative vibrational assignments, is present in Table 1. Selected calculated normal modes corresponding to strong and moderate intensity bands are illustrated in Figure 4 (see Table S2 for all the normal modes). The excellent agreement between the relative intensity of the experimental data with the calculated spectrum, indicates that in the solid state, 5-HTP is in a zwitterionic form, as observed in previous studies.[68] Additionally, the overall spectral profile of 5-HTP more closely resembles that of 5-HT than Trp.[35] This is attributable to the presence of the hydroxyl group at the C11 position of the benzene ring, a structural similarity shared by 5-HTP and 5-HT.

The dominant bands in the solid-state normal Raman spectrum of 5-HTP appear at 1346, 1427, and 1553 cm^{-1}, which have contributions mainly from the in-plane ring vibrations. The 1346 cm^{-1} band results from a combination of in-plane indole ring C−C stretch, C−H bend, and N−H bend coupled to C20−H25, H21−C16−H22 bend along with the bending vibration of the amino group. The 1427 cm^{-1} band is assigned to a combination of in-plane C3−N14 stretch, C7−N14−C9 bend, C7−N14−H15 bend, and C10−C4−H6 bend. The intense band at 1553 cm^{-1} is predominantly assigned to the C7−C9 stretching of the pyrrole ring, with minor contribution from C16−C9 stretch, C3−C10 stretch, and C10−C4−H6 bend. Similar intense bands are observed in the spectra of Trp and 5-HT, with the corresponding band in the latter slightly shifted to 1546 cm^{-1}.[33−35] The small shift relative to Trp is expected due to the localized nature of the C7−C9 vibration, which may be minimally affected by the hydroxyl substitution at the benzene ring.

In Trp, the Raman band near 1550 cm^{-1} has been used as a conformational marker in proteins due to its correlation with the absolute value of the dihedral angle C9 = C7 − C(α) − C(β).[70] While this correlation has not been established for 5-HTP, the optimized structure (Figure 1) exhibits a dihedral angle of 109°, consistent with the values reported for Trp.[33,70] This suggests a similar conformational structure and the potential application of this band as a marker for probing the 5-HTP structure.

In the normal Raman spectrum, medium-intensity bands are also observed at 496/501, 764, 929/935, 1236, and 1312 cm^{-1}, involving a combination of in-plane indole ring and main chain vibrations. The 496/501 cm^{-1} band is assigned to indole ring bend, C1−C2 stretch, and H21−C16−H22 bend. The 764/773 cm^{-1} band is associated with C3−C10−C4 bend, C7−N14−C3 bend, and C2−C1−C11 bend in the indole ring, C4−C11 stretch, H22−C26−H20 bend, and vibrational bending in the carboxylate and the α-carbon (C20) groups. The 929/935 cm^{-1} peaks involve C20−C16 stretch and bending vibrations of the β-carbon and amino groups. The peak at 1236 cm^{-1} corresponds to bending movements in the α-carbon group and indole. The band at 1312 cm^{-1} is assigned primarily to C11−O13−H5 bend, H19−N17−H28 bend, H22−C16−C9−C7 torsion, and H25−C20−C24−C23 torsion.

Additionally, several out-of-plane indole ring modes are also identified at 436, 457, 461, 749, 834, and 861 cm^{-1}. The bands at 436 and 749 cm^{-1} have the contribution of O13−C1−C4−C11 torsion and N14−C10−C2−C3 out-of-plane, respectively. The bands at 457 and 461 cm^{-1} involve H15−N14−C3−C10 out-of-plane, whereas the peak at 834 cm^{-1} is assigned to H8−C7−C9−C16 out-of-plane and H12−C1−C2−C9 out-of-plane. The peak at 861 cm^{-1} combines C9−C7−H8 out-of-plane and H12−C1−C2−C9 torsion.

To the best of our knowledge, the SERS spectrum of 5-HTP has not been previously reported. Figure 5 shows the SERS spectra of 5-HTP obtained at various concentrations by using silver nanoparticles. In comparison with the normal Raman spectrum, the SERS spectra are broader, with noticeable differences in the relative band intensities. The spectral deconvolution for the 100 μM SERS spectrum is shown in Figure S1, and the band positions are also summarized in Table 1. No major shifts in band positions are observed between the SERS and normal Raman spectra, except for a few bands, such as the 1553 cm^{-1} band blueshifting to 1569 cm^{-1} in SERS. However, significant changes in the relative intensity are observed.

The most prominent SERS bands occur at 487, 1246, 1328, and 1640 cm^{-1}, while medium-intensity bands are observed at 466, 518, 821, 841, 1234, 1288, 1343, 1455, and 1569 cm^{-1}. Additionally, other medium-intensity bands are also observed in the 1000−1100 cm^{-1} region, which were absent or very weak in the normal Raman spectrum. Several weak and very weak bands in SERS also occur at 407, 593, 1122, and 1429 cm^{-1}. Bands in the 700−780 cm^{-1} region, which are moderately intense in the normal Raman spectrum, are weak or absent in SERS. Similarly, the band at 929/935 cm^{-1} in the normal Raman spectrum becomes weaker in SERS. Interestingly, the most intense band in the normal Raman spectrum at 1427 cm^{-1} is weak in the SERS spectrum, whereas the band at 1553 cm^{-1} exhibits medium intensity and upshifts to 1569 cm^{-1}.

The SERS spectrum depends on the molecule adsorption geometry and the conformation on the nanoparticle surface. The decrease in the relative intensity of the in-plane ring bands at 1429 and 1569 cm^{-1}, along with the enhancement of several

https://doi.org/10.1021/acs.jpcc.5c06154
J. Phys. Chem. C 2025, 129, 20313−20326

Table 1. Band Position of the Experimental Normal Raman of Solid 5-HTP and SERS Spectrum (100 μM), Together with the Calculated Frequencies (with and without Scaling Factor), Raman Activity, and Normal Mode Assignments[a]

exp. freq. (cm^{-1}) NR	exp. freq. (cm^{-1}) SERS	calc. freq. (cm^{-1})	scaled calc. freq. (cm^{-1})	Raman activity ($Å^4$/amu)	assignments
206		223.1	216.5	2.2	δC16H21H22, τH18N17C20C16, τH18N17C20C16, δC24C20N17
234		225.8	219.0	0.8	τH18N17C20C16, τH28N17C20C16
266		282.2	273.7	1.6	γC11O13H5, τH5O13C11C1
		317.3	307.8	1.5	γC11O13H5, τC3C10C4C11, γN14C10C2C3, τC9C7N14C3, γC2C1H12, δN17C20C16
329		327.3	317.5	2.0	δC24O23O26, δC24C20N17, τH19N17C20C16
357		376.0	364.7	1.1	δC3N14H15, δC9C7H8, δ 13C11C4, τC2C1C11C4
387		385.9	374.3	1.4	δC11O13H5, δC16H21H22, δN17H18H19, δN17C20C16
407	408	417.1	404.6	4.0	γC9C7H8, γC2C1H12, γC11O13H5, δN17C20C16, δH21C16H22, τH15N14C3C10
436	442	435.7	422.7	3.0	τH27C10C4C11, τC3C10C4C11, τC2C1C11C4, τC7N14C3C10, γO13C1C4C11
457	466	454.7	441.1	7.0	δC3C10C4, γH15N14C3C10
461	466	460.0	446.2	7.5	γH15N14C3C10
496/501	487	503.0	487.9	10.1	δH21C16H22, δC11C4O13, νC2C1, δC2C1C11, δN14C3 C2, δC16C9C7
518/535	518	535.7	519.6	2.2	δH21C16H22, νN17C20, δO26C24O23, δO23C24C20
593	594	595.3	577.5	8.3	δH22C16H21, γC9C7H8, νC3C10, δN14C3C2, δO13C11C4
601/609	614	612.9	594.5	0.9	τH6C4C11C1, τC9C7N14C3, τC3C10C4C11, τO13C1C4C11
645		655.0	635.3	5.4	τC9C7N14C3, γO13C1C4C11, γC16C7C2C9
662	665	689.1	668.4	7.4	δC10C4C11, δC7N14C3, δN17C20C24, νC16C9, δO26C24O23, δO23C24C20
707/721		709.6	688.3	9.8	γN14C7H8, γC11C1H12, γC3C10H27, γC11C4H6, δC20C16C9, γO26C20O23C24
749		760.3	737.5	1.8	δH22C16H21, τC1C11C4C10, τC3C10C4C11, τC2C1C11C4, γN14C10C2C3
764		774.4	751.2	31.1	δC3C10C4, δC2C1C11, δH22C16H21, νC11C4, δC7N14C3, γO26C20O23C24
773		805.1	780.9	24.6	γC9C7H8, γH27C10C27H6, δH22C16H21, δH18N17H28, δO26C24O23, δC1C11C4, γO26C20O23C24
806	798	816.5	792.0	7.6	γH6C4C11C1, γH27C10C4C11
826	821	845.8	820.4	20.7	δH22C16H21, νN17C20, τH8C7C9C16
826	821	850.3	824.8	20.3	δC3N14C7, δC1C11C4, γH8C7C9C16
834	841	872.5	846.3	17.6	δH22C16H21, δH18N17H19, νN17C20, γH12C1C2C9, γH8C7C9C16
861	858	879.9	853.6	8.0	γC9C7H8, δH18N17H19, γH12C1C2C9
		906.1	878.9	6.1	δH22C16H21, νC24C20, δO26C24O23, τH19N17C20C16
929/935	918	950.1	921.6	35.8	δH22C16H21, νC20C16, τH28N17C20C16
943		957.0	928.3	2.9	τH6C4C11C1, τH27C10C4C11
957/970	952	964.9	936.0	26.9	δC4C10H27, δH22C16H21, δH18N17H19, νC1C11, νC11C4, δC7N14C3
1026	1017	1060.8	1028.9	22.7	δC2C1H12, δC10C4H6, δC7N14H15, δH22C16H21, νN17C20
1047	1042	1065.7	1033.7	5.8	δC2C1H12, δC4C10H27, δC7N14H15, τH19N17C20C16
1059	1070	1097.1	1064.2	12.8	δC2C1H12, δC10C4H6, δH21C16C9, τH18N17C20C16
1094	1094	1114.5	1081.0	2.3	δC10C4H6, νN14C7, δH15N14C7, δH8C7C9
1122	1122	1136.9	1102.8	17.3	νC20C16, δH25C20C24, τH19N17C20C16, τH28N17C20C16
1131		1156.8	1122.1	13.9	δN14C7H8, νC10C4, δH6C4C10, δH27C10C4
1179	1176	1198.6	1162.6	16.0	δC3C10H27, νC1C11, δH5O13C11, δH12C1C2
1199	1191	1235.1	1198.1	21.0	δC11C4H6, δC11C1H12, δC3N14H15, δC9C7H8, δH22C16H21, νC20C16, δH18N17H19, νO13C11, δH5O13C11
1216		1248.7	1211.2	41.2	νO13C11, δC3C10H27, δN14C7H8, νC16C20, δH18N17H19, δH12C1C2, δH25C20C24
1229		1263.4	1225.5	4.4	δC4C10H27, νN14C7, τH22C16C9C7
1236	1234	1273.1	1234.9	50.8	δC2C1H12, δC11O13H5, δC4C10H27, δH18N17H28, δH15N14C7, δH8C7C9, δH25C20C24
1260	1246	1295.1	1256.2	51.3	νC11O13, δH19N17H28, δH27C10C4, δH21C16C9, τH22C16C9C7
1297	1288	1336.4	1296.3	66.6	δC11C1H12, δH22C16H21, δ 19N17H28, νN14C7, νN14C3, νO13C11
1312	1328	1359.4	1318.6	25.3	δC11O13H5, δH19N17H28, τH22C16C9C7, τH25C20C24O23
		1370.6	1329.5	21.1	δC10C4H6, δC11C1H12, δC9C7H8, δH22C16H21, δH19N17H18, δH5O13C11, τH25C20C24O23

https://doi.org/10.1021/acs.jpcc.5c06154
J. Phys. Chem. C 2025, 129, 20313−20326

Table 1. continued

exp. freq. (cm^{-1}) NR	exp. freq. (cm^{-1}) SERS	calc. freq. (cm^{-1})	scaled calc. freq. (cm^{-1})	Raman activity (Å^4/amu)	assignments
1346	1343	1386.3	1344.7	213.8	δC9C7H8, δC3N14H15, δH22C16H21, νC20C16, νC2C1, δH6C4C10
1352		1393.7	1351.9	58.8	δC11O13H5, δN14C7H8, νC10C4, τH21C16C9C7, τH25C20C24O23
1392		1417.1	1374.6	8.6	δH18N17H28, νO26C24, νO23C24, τH25C20C24O23
1404		1450.1	1406.6	30.2	νO26C24, δH18N17H28, δH19N17H18, δH28N17H19
1427	1429	1467.7	1423.7	282.2	δC10C4H6, νN14C3, δC9C7N14, δH15N14C7
1445	1455	1477.1	1432.8	12.3	δH22C16H21
1469	1455	1497.7	1452.8	29.0	δC10C4H6, δC3N14H15, νC7N14, δH12C1C2, δH27C10C4
1488	1502	1555.5	1508.9	13.8	δC11C4H6, δC11O13H5, δC3N14H15, δN14C7H8, νC1C11, νC2C1, δN14C3C2
	1529				
1553	1569	1611.2	1562.8	254.5	δC10C4H6, νC10C3, νC9C7, νC16C9
		1622.5	1573.8	8.8	δH18N17H28, δH19N17H18, δH28N17H19
1591	1597	1652.6	1603.0	61.2	δC11O13H5, δC3N14C7, νC7C9, νC2C1, νC11C4, δC3C10C4
		1664.0	1614.1	13.2	δH18N17H28, δH19N17H18, δH28N17H19, τH19N17C20C16
1624	1630	1706.8	1655.6	42.1	νC1C2, δC11O13H5, νC10C4, δC11C4H6, δC7N14H15, νC1C11, νC10C4, νC3C10, νC2C1
	1640	1712.1	1660.7	8.3	δC24C20H25, δH18N17H28, νO26C24, νO23C24

[a]For the description of the vibrational modes, the atom numbering in Figure 2 was used with the following abbreviations: stretching (ν), bending (δ), torsion (τ), and out-of-plane bending (γ).

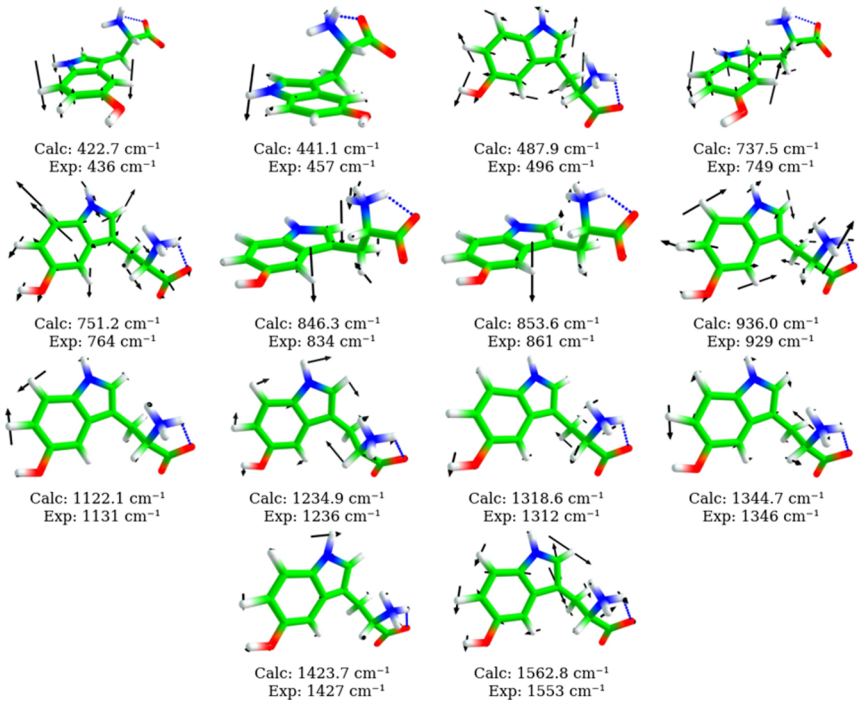

Figure 4. Selected 14 normal modes of 5-HTP with their respective DFT-calculated (scaled with factor 0.97) and experimental frequencies. The arrows indicate atomic displacements.

ring out-of-plane modes suggests that the indole ring may adopt a tilted orientation relative to the silver surface.[34,58,71] The intense band at 1640 cm^{-1} in SERS, absent in the normal Raman spectrum, corresponds to a low Raman activity mode at 1660.7 cm^{-1} in the DFT calculation involving carboxylate stretching and amino vibrations. From previous studies of Trp, Phe, and other amino acids,[16,25,34,72,73] enhancement is indicative that 5-HTP may strongly interact with the surface, likely through the carboxylate coordination to silver atoms.[27,71,73,74] The presence of bands at 518/535 cm^{-1} in SERS associated with carboxylate vibrations supports this interpretation.

Other enhanced SERS bands correspond to complex vibrational modes involving both the ring and the main chain. Given the interplay of the chemical and electromagnetic enhancement mechanisms that influence the relative intensity of 5-HTP, we further investigate the adsorption behavior by carrying out a combination of MD simulations and DFT calculations.[74,75] MD simulations were performed by using both neutral and charged silver layers. Figure 6 shows the initial randomly distributed and final configurations after 200 ns, showing a direct interaction between several 5-HTP molecules and the metal surfaces. Small aggregates of 5-HTP molecules are also observed, influenced by intermolecular interactions including hydrogen bonding. Representative

https://doi.org/10.1021/acs.jpcc.5c06154
J. Phys. Chem. C 2025, 129, 20313−20326

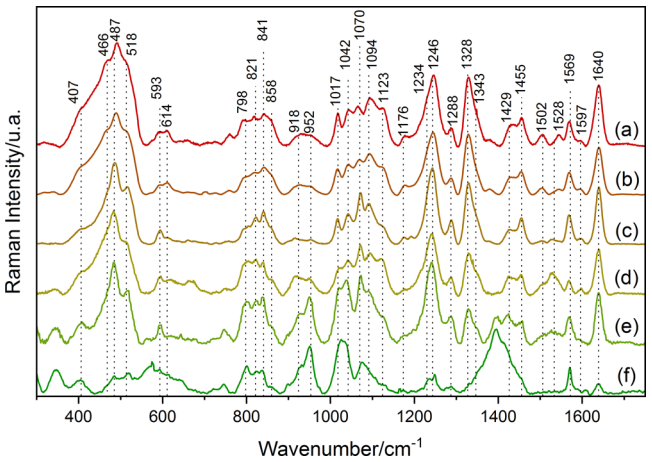

Figure 5. SERS spectra of 5-HTP at different concentrations at pH7 (a) 1 mM; (b) 500 μM; (c) 100 μM; (d) 50 μM; (e) 10 μM, and (f) 1 μM. The spectra were obtained with silver nanoparticles prepared by the Lee−Meisel method and recorded with 785 nm excitation wavelength. Sodium nitrate was used as an aggregating agent.

surface-bound conformations of some 5-HTP molecules at the neutral and charged metal layers are shown in Figure 7. In both cases, 5-HTP does not adopt a single preferential orientation. On the neutral surface, the aromatic ring is generally oriented nearly parallel to the surface, with minimal direct contact between the amino/carboxylate groups and the metal surface. However, in some cases, the ring is perpendicular or tilted, and the amino and carboxylate groups approach or directly interact with the surface. In one case, 5-HTP interacts directly with the surface through the ring in a tilted configuration. On the charged silver surface, the 5-HTP molecules preferentially interact with the carboxylate group, and the indole ring typically adopts a tilted or parallel geometry. A few molecules adopt a geometry directly interacting through the ring, and others are also adsorbed with similar configurations to those observed in the neutral layer. The variability in adsorption conformations revealed by MD simulations may explain the spectral broadening observed in the SERS spectra and supports the interpretation that 5-HTP predominantly adsorbs with its indole ring tilted or parallel, and the carboxylate group acts as the main anchoring moiety. This computational result also explains the presence of very few pure indole ring in-plane vibrational bands in the SERS spectrum and the enhancement of vibrational modes with a significant carbonyl stretching character.

The analysis of the MD results provides valuable information about the molecular orientations. In the case of 5-HTP, the orientation of the indole ring adsorbed on the silver surface could greatly affect the SERS signal. Figure 8 shows the angles of the vectors defined by the indole ring atoms C9−C4 of 5-HTP molecules relative to the normal of the silver surface.

As can be seen, on the neutral silver surface, the indole rings form an average angle of approximately 90° with respect to that of the normal, indicating that the indole ring is nearly parallel to the surface. However, for the charged surface, in addition to the parallel configurations, new possible adsorption geometries are also observed with angles of 40−60° and 120−140°, indicating the occurrence of tilted conformations for some 5-HTP molecules. In Figure 9, the analysis of the dihedral angle (C7−C9−C16−C20) reflects the main chain conformations relative to the indole moiety of 5-HTP in proximity to the silver surface. In the neutral layer, the dihedral angle distributions of the nearest 5-HTP molecules oscillate between approximately −110° and −60° and 60° to 120°. In the charged layer, the angles vary from −130° to −90° and 60° to 120°. For the more distant molecules, the probabilities tend to converge to ∼100°, consistent with the angle shown in Figure 2 for the normal Raman spectrum.

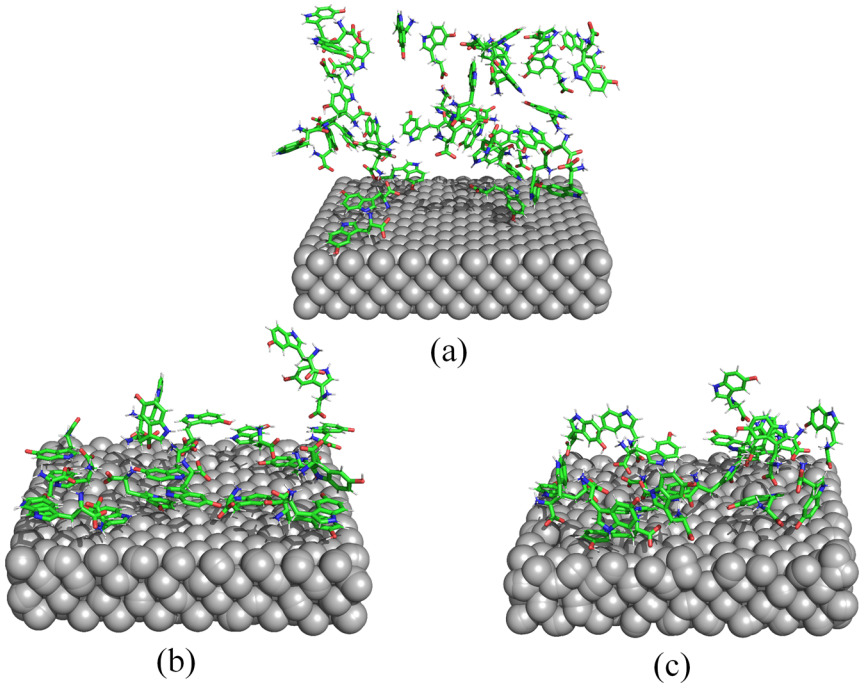

Figure 6. Snapshots of the (a) initial and last configurations of the 200 ns MD simulations obtained with a (b) neutral layer and (c) charged layer.

https://doi.org/10.1021/acs.jpcc.5c06154
J. Phys. Chem. C 2025, 129, 20313−20326

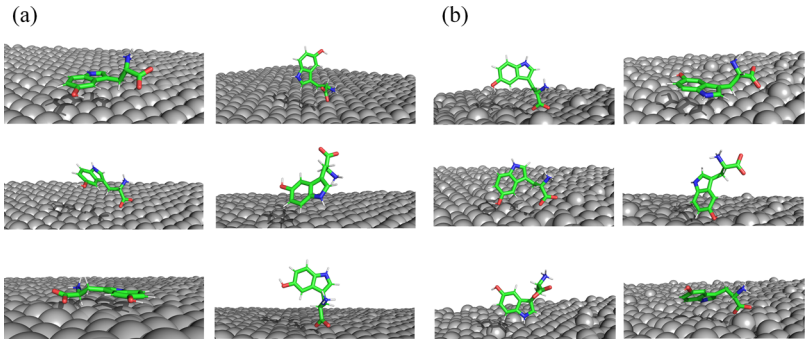

Figure 7. Snapshot from the last configuration of the 200 ns MD simulations showing the main configurations of 5-HTP molecules on the (a) neutral and (b) charged surfaces.

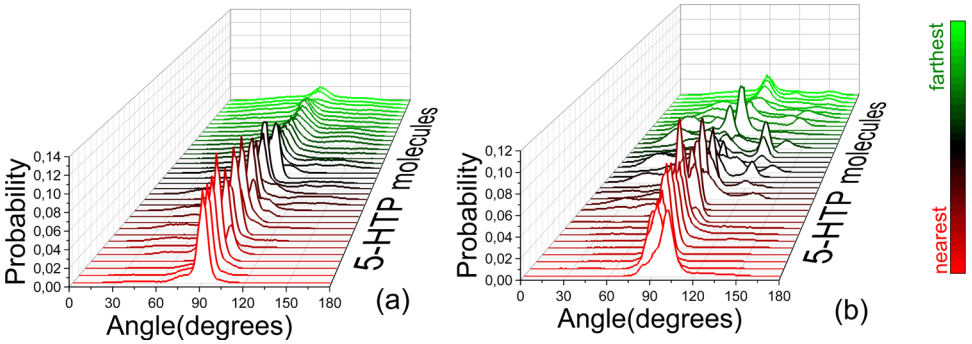

Figure 8. Angle histograms of the vector formed by the C9−C4 bond of 5-HTP with respect to the normal vector of the surface on the (a) neutral layer and (b) charged layer silver surfaces. The color bar indicates the molecular proximity to the surface, starting from red (nearest) to green (farthest). The axis perpendicular to the page corresponds to the same proximity scale used in the color bar.

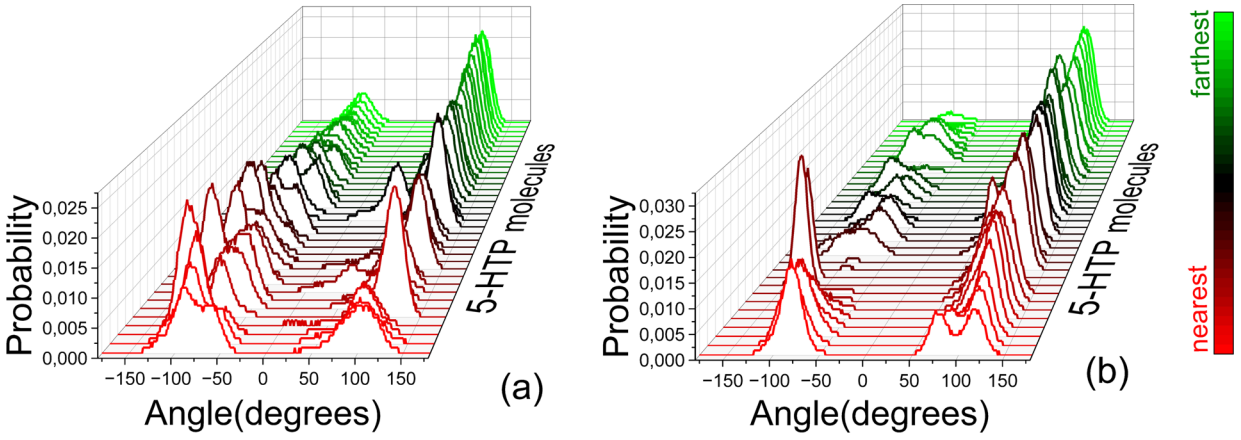

Figure 9. Histograms with the values of the C7−C9−C16−C20 dihedral angle of 5-HTP molecules on the (a) neutral layer and (b) charged layer silver surfaces. The color bar indicates the molecular proximity to the surface, starting from red (nearest) to green (farthest). The axis perpendicular to the page corresponds to the same proximity scale used in the color bar.

These results highlight the influence of the silver surface charge on the adsorption geometry of 5-HTP and its impact on the observed SERS spectra. The predominance of parallel orientations on the neutral surface suggests interactions between the indole π-system and the metallic surface. In contrast, the broader range of tilt angles observed for the charged surface indicates that electrostatic interactions between the metal atoms and the carboxylate and amino groups of 5-HTP can lead to additional adsorption geometries. These MD simulation results provide a structural basis for understanding the intensity enhancement observed in SERS. At the neutral silver surface, the predominance of parallel indole orientations favors the enhancement of out-of-plane ring vibrations, in agreement with the bands observed in the SERS spectra. In contrast, the charged surface promotes additional tilted configurations, allowing for the enhancement of both in-plane and out-of-plane vibrational modes. This explains the relative intensity differences observed in the normal Raman and SERS spectra.

To elucidate the origins of the spectral enhancement in the SERS spectra, we performed DFT calculations by explicitly including only ten silver atoms in the vicinity of the 5-HTP molecule, whereas the remaining silver atoms of the surface were omitted. For that, four representative configurations

https://doi.org/10.1021/acs.jpcc.5c06154
J. Phys. Chem. C 2025, 129, 20313−20326

obtained from the MD simulations, sampling distinct interaction modes of 5-HTP with the surface, were selected as the initial geometries for DFT calculations. Configurations 1 and 2, referred to here as Models 1 and 2, correspond to conformations commonly observed in the neutral layer. In contrast, Models 3 and 4 were derived from configurations representative of the charged layer (total system charge of +1), where stronger electrostatic interactions are present.

The optimized structures of the four models are shown in Figure 10 with the atomic coordinates listed in Tables S3 and S6 and their electronic energies included in Table S7. As can be seen, in Models 1 and 3, the indole ring of 5-HTP is tilted with respect to the silver surface, while in Models 2 and 4, it lies nearly parallel to the surface.

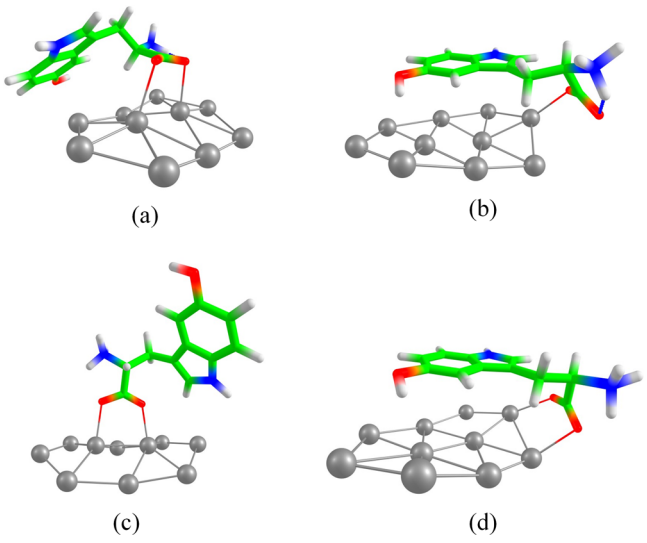

Figure 10. Optimized structures of 5-HTP−Ag clusters from DFT calculations at the M06-2X/6-311++G(d,p)/LANL2DZ level of theory: (a) Model 1 (b) Model 2, (c) Model 3, and (d) Model 4. Models 1 and 2 correspond to neutral silver surfaces. Models 3 and 4 correspond to charged silver surfaces.

Figure 11 shows the comparison between the experimental SERS spectrum at 100 μM and the calculated Raman spectra of the four structural models (Tables S8−S11).

As shown, several discrepancies exist between the predicted Raman intensities and the experimental SERS signal, which is expected given that the theoretical calculation primarily accounts for the chemical effect contribution but not for the electromagnetic enhancement. The latter is strongly dependent on the molecular adsorption geometry of the metallic surface. Models 2, 3, and 4 predict a high Raman active normal mode near 1640 cm^{-1}, involving carboxylate stretching coupled with amino group vibrations. This band is absent in the normal Raman spectrum of solid 5-HTP and shows a low calculated intensity in the absence of metal atoms. This suggests that its enhancement arises from the direct interaction between 5-HTP and the silver atoms. In these models, the molecule is coordinated to the silver atoms via the oxygen atoms of the carboxylate group. Interestingly, unlike Model 1, Models 2 and 3 reproduce well the experimental relative intensity ratio between the 1640 and 1569 cm^{-1} bands. Furthermore, these models also predict strong bands at 510 cm^{-1} (Model 1), 498 cm^{-1} (Model 2), 542 cm^{-1} (Model 3), and 491 cm^{-1} (Model 4), respectively, which correlate with the experimental SERS band at 518 cm^{-1}. These modes involve vibrational contributions from the main chain and the carboxylate group, including H21−C16−H22 bend and the O23−C24−O26 bend. Based on these results, it can be inferred that under the used experimental physicochemical conditions, 5-HTP exhibits a strong interaction with silver atoms through the COO^- group, suggesting the prevalence of monodentate or bidentate coordination geometries. This result aligns with previous SERS studies of Trp, where the carboxylate group has been identified as the binding site to the silver surface.[31,58,69−72] For instance, Aliaga et al.[58] reported the SERS spectrum of zwitterionic Trp adsorbed on silver nanoparticles at neutral pH, suggesting that the molecule interacts primarily through the carboxylate group, while the amino group remains in proximity to the metal surface. Similarly, the SERS analysis by Chuang et al.[71] and Maiti et al.[31] also indicates that this amino acid preferentially interacts with the silver surface via both the carboxylate and amino groups.

Several bands, mainly associated with hydrogen out-of-plane vibrational modes of the aromatic ring, are observed at 798, 841, and 858 cm^{-1} in the SERS spectrum. Similarly, the SERS bands observed at 442 and 466 cm^{-1} correspond to CH and NH out-of-plane deformations in the ring. Models 2 and 3 also predict intense Raman bands in the 800−900 cm^{-1} region. The enhancement of these out-of-plane modes suggests that the aromatic ring does not adopt a perpendicular orientation relative to the silver surface but rather a tilted or parallel configuration. This interpretation is consistent with the structural configurations proposed by Models 2 and 3. The observed enhancement also implies a significant interaction between the aromatic ring and the metal surface. This result is supported by the work of Aliaga et al.,[58] which used MD simulations to investigate the SERS spectrum of Trp, and concluded that the indole ring lies parallel or, at minimum, tilted relative to the Ag surface.

Similar SERS behavior has been reported for Trp, where π−electron−metal interactions and metal coordination significantly influence the observed spectral enhancements.[35,76,77] The interpretation that 5-HTP may adopt a tilted adsorption geometry is in agreement with the observation that the ring in-plane vibration band at 1429 cm^{-1}, which is the most intense in the normal Raman spectrum, exhibits a marked decrease in intensity in the SERS spectrum. Previous SERS studies of 5-HT have also shown that depending on the physicochemical conditions the aromatic ring can interact directly with the metal surface in either a parallel or tilted orientation.[34,35]

All models predict weak Raman bands in the 1000−1100 cm^{-1} spectral region. Therefore, the SERS enhancement observed in this region is likely dominated by the electromagnetic contribution. Notably, the three bands at 1017, 1042, and 1070 cm^{-1} arise from vibrational modes involving the main chain with significant contributions from the amino group. Considering the interaction via coordination of the COO^- group, even though the amino group does not directly coordinate with the metal, its special proximity to the surface may facilitate the enhancement of these vibrational modes. For example, in Models 1, 2, 3, and 4, the nitrogen atom of the amino group lies approximately 3.69, 5.06, 5.08, and 4.42 Å, respectively, from the nearest silver atom. Thus, considering that the most substantial enhancement typically occurs for atomic groups placed within ∼1 nm of the surface, the observed intensity of these amino group Raman bands is consistent with this spatial arrangement.[14,15] Therefore, results

https://doi.org/10.1021/acs.jpcc.5c06154
J. Phys. Chem. C 2025, 129, 20313−20326

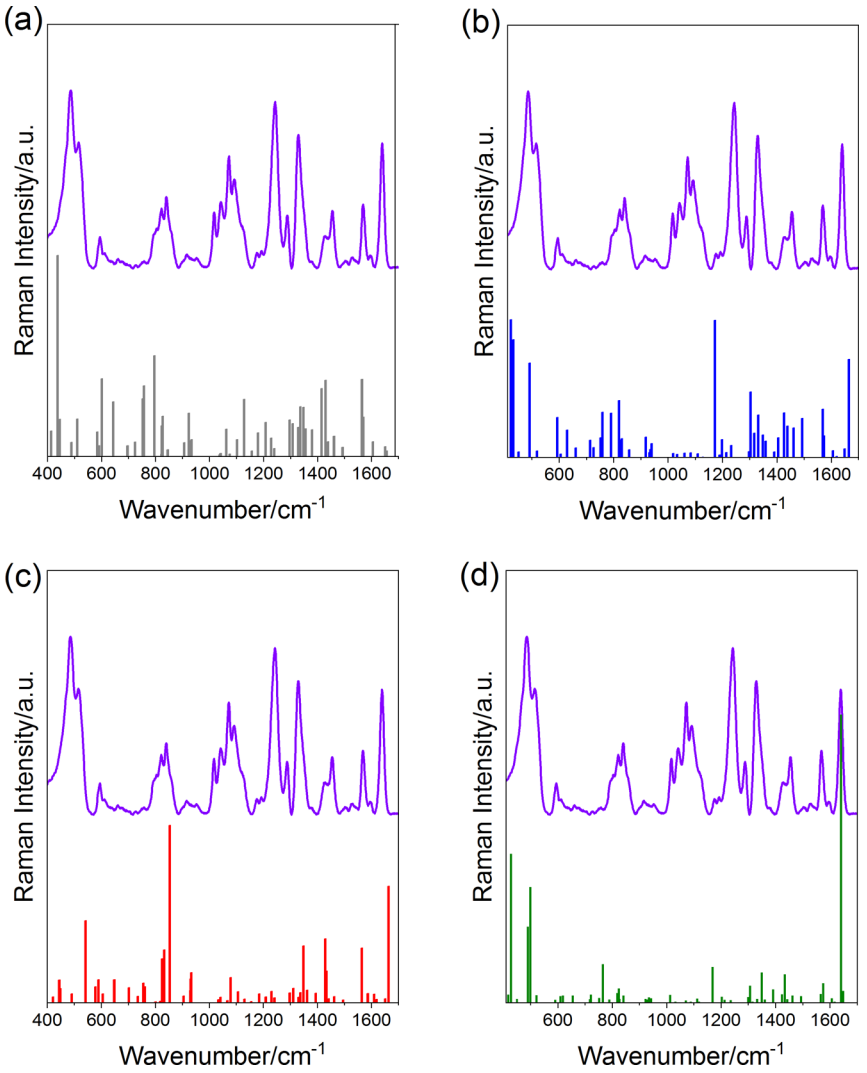

Figure 11. Comparison between the experimental SERS spectrum of 5-HTP at 100 μM concentration (solid line) and DFT-calculated (frequency-scaled by 0.97) Raman spectra of (a) Model 1, (b) Model 2, (c) Model 3, and (d) Model 4.

indicate that the amino group resides close to the metallic surface and may play a key role in the adsorption behavior of 5-HTP. This interpretation is also supported by the findings of Aliaga et al.,[58] Chuang et al.,[71] and Maiti et al.[31] for Trp, which proposed that the main chain, including the amino group, is placed near the silver surface.

All of the computational models also failed to predict intense Raman bands experimentally observed at 487 and 1234/1246 cm^{-1}. On the other hand, only Model 3 predicts a band of medium intensity near 1327 cm^{-1}. Thus, it is more likely that the enhancement of these bands arises primarily from the electromagnetic contribution to the SERS effect. The intense Raman band at 487 cm^{-1} is assigned to in-plane ring deformation, coupled with the bending vibrations of H21−C16−H22. The band at 1234 cm^{-1} is predominantly a ring in-plane vibration with minor contribution from the H25−C20−C24 bend. The 1246 cm^{-1} band also involves ring in-plane vibration, with additional contributions from the bending of the amino and H21−C16−C9 atomic groups. In the normal Raman spectrum, the band at 1236 cm^{-1} is more intense than that at 1260 cm^{-1} (1246 cm^{-1} in the SERS spectrum). However, in SERS the situation is reversed with the band at 1246 cm^{-1} becoming one of the most intense characteristics in the spectrum. Similar interpretations can be proposed for the bands at 1328 and 1343 cm^{-1}. In the normal Raman spectrum, the 1346 cm^{-1} band appears to be slightly more intense than that at 1328 cm^{-1}. The band observed at 1328 cm^{-1} corresponds to a ring in-plane vibrational mode with some contribution from backbone vibrations. However, the band at 1328 cm^{-1} also exhibits coupling with the amino group, whereas the peak at 1343 cm^{-1} does not. This distinction may account for the difference in the relative intensities observed between the normal and SERS spectra, considering that the amino group may be positioned close to the metal surface. Nevertheless, a definite explanation for the selective enhancement of these bands remains uncertain. If the molecule adopts a perpendicular or tilted orientation relative to the surface, then enhancement of these vibrational modes would be expected. Since these modes also involve contributions from the main chain, the proximity of these atomic groups to the surface would further facilitate their SERS enhancement.

The small variations in the SERS intensities observed at concentrations above 1 μM suggest that surface adsorption sites on the Ag nanoparticles become saturated, leading to a nearly constant distribution of the adsorption geometries. At 1 μM, the SERS spectrum exhibits interference from the citrate

https://doi.org/10.1021/acs.jpcc.5c06154
J. Phys. Chem. C 2025, 129, 20313−20326

molecules used as capping agents, preventing accurate interpretation of the 5-HTP vibrational bands (see Figure S2). Nevertheless, some differences in the relative intensities of the 5-HTP SERS bands above 1500 cm^{-1} are observed in comparison to higher concentrations, possibly indicating subtle adjustments in adsorption geometry. For example, the relative intensities of the bands at 1569 and 1640 cm^{-1} differ, with respect to those at higher concentrations. Still, the presence of the carbonyl stretching band demonstrates that, even at this concentration, the carboxylate group remains involved in the coordination to the silver surface. The relative intensity profile in this spectral region matches closely with the calculated spectrum from Model 1, further supporting the conclusion that the adsorption occurs through the carboxylate group.

The band observed at 1553 cm^{-1} in the normal Raman spectrum exhibits a blue shift to 1569 cm^{-1} in SERS. Considering previous Raman studies of Trp, this shift may be attributed to differences in the dihedral torsional angle between the 5-HTP molecule in the solid state and when adsorbed on the silver surface. Such spectral behavior can be explained by the tilted adsorption geometry and configuration adopted on the surface due to the influence of interactions involving the aromatic ring and carboxylate groups with the silver surface. For example, the DFT-optimized geometries of Models 2, 3, and 4, exhibit dihedral angles of −9.93°, −88.27°, and 6.86°, respectively, which are different from the optimized geometry of 5-HTP without metal coordination. Coordination through the carboxylate group, along with π-interaction between the indole ring and the surface, may affect this dihedral angle, which can result in the observed blueshift of the band.

Interestingly, a SERS investigation of 5-HT by Manciu et al.[35] using silver as the SERS substrate suggested the potential formation of a planar adsorption geometry relative to the silver surface, whereas Song et al.[34] proposed a tilted orientation of the indole ring with respect to the surface. Analogous interpretations have been reported for Trp: for example, Aliaga et al.[58] proposed a configuration in which the pyrrole moiety adopts a tilted (nearly parallel) orientation relative to the surface, while Maiti et al.[31] suggested a nearly perpendicular configuration. These findings highlight the possibility of multiple adsorption modes for these molecules. Since 5-HTP shares structural characteristics with both 5-HT and Trp, the coexistence of different adsorption conformations suggested for 5-HTP with the aromatic ring oriented either parallel or tilted with respect to the silver surface seems to be plausible.

CONCLUSIONS

In this work, we have characterized the normal Raman and SERS spectra of 5-HTP using a combined approach with classical MD simulations and DFT calculations. The DFT-calculated spectrum is in excellent agreement with the experimental normal Raman data and confirms that 5-HTP exists in its zwitterionic form in the solid state. On the other hand, the SERS spectra revealed significant changes in band intensities and frequencies in comparison with the normal Raman spectrum of the solid. It is particularly the emergence of strong bands associated with the carboxylate and amino groups, suggesting the direct interaction of these moieties with the silver surface. The MD simulation results indicated that 5-HTP does not adopt a single conformation on the nanoparticle surface but mainly binds through the carboxylate group with the ring in tilted or parallel orientations. These main configurations were further validated through DFT calculations on small clusters of silver atoms. The calculation in different models demonstrates that incorporating carboxylate-metal coordination and ring-surface interactions best reproduces the experimental SERS data. Overall, the obtained results elucidate the orientation and interaction mechanisms of 5-HTP at the silver nanoparticle interfaces and highlight its potential applications as a site-specific Raman probe in protein and 5-HT metabolism sensing, offering a complementary tool to fluorescence for probing biomolecular environments.

ASSOCIATED CONTENT

Supporting Information

The Supporting Information is available free of charge at https://pubs.acs.org/doi/10.1021/acs.jpcc.5c06154.

Figures presenting spectral deconvolution, the SERS spectra of 5-HTP and aggregated AgNPs. Tables provide the data from DFT calculations, comprising the Cartesian coordinates of the optimized structures, calculated vibrational frequencies, Raman activities, normal mode, as well as the electronic energies and dipole moments of the adsorption models (PDF)

AUTHOR INFORMATION

Corresponding Author

Erix Alexander Milán-Garcés − *Departamento de Física Geral, Instituto de Física, Universidade de São Paulo, 05508090 São Paulo, SP, Brazil;* orcid.org/0000-0003-1134-7184; Email: garces@usp.br

Authors

Caio Hiroaki Miyake − *Departamento de Física Geral, Instituto de Física, Universidade de São Paulo, 05508090 São Paulo, SP, Brazil*

Jayr Henrique Marin − *Departamento de Química Fundamental, Instituto de Química, Universidade de São Paulo, 05508-900 São Paulo, SP, Brazil*

Gabriel Conishi Cardozo − *Departamento de Física Geral, Instituto de Física, Universidade de São Paulo, 05508090 São Paulo, SP, Brazil;* orcid.org/0009-0007-9982-0509

Diogo Soga − *Departamento de Física Geral, Instituto de Física, Universidade de São Paulo, 05508090 São Paulo, SP, Brazil*

Evandro Luiz Duarte − *Departamento de Física Geral, Instituto de Física, Universidade de São Paulo, 05508090 São Paulo, SP, Brazil;* orcid.org/0000-0001-5550-6541

Antonio Rodrigues da Cunha − *Universidade Federal do Maranhão, 65800-000 Maranhão, Brazil;* orcid.org/0000-0002-6280-8772

Rômulo Augusto Ando − *Departamento de Química Fundamental, Instituto de Química, Universidade de São Paulo, 05508-900 São Paulo, SP, Brazil;* orcid.org/0000-0002-3872-8094

Complete contact information is available at: https://pubs.acs.org/10.1021/acs.jpcc.5c06154

Funding

The Article Processing Charge for the publication of this research was funded by the Coordenacao de Aperfeicoamento de Pessoal de Nivel Superior (CAPES), Brazil (ROR identifier: 00x0ma614).

Notes

The authors declare no competing financial interest.

■ ACKNOWLEDGMENTS

This research was supported by the São Paulo Research Foundation (FAPESP), the National Council for Scientific and Technological Development (CNPq) and the Brazilian Federal Agency for Support and Evaluation of Graduate Education (CAPES). C.H.M. acknowledges support from a CNPq fellowship. Computational resources were provided by the High-Performance Computing (HPC) facilities of the Superintendence of Information Technology at the University of São Paulo.

■ REFERENCES

(1) Duerschmied, D. Role of Platelet Serotonin in Innate Immune Cell Recruitment. *Front. Biosci.* **2019**, *24* (3), 514−526.
(2) Maffei, M. E. 5-Hydroxytryptophan (5-HTP): Natural Occurrence, Analysis, Biosynthesis, Biotechnology, Physiology and Toxicology. *Int. J. Mol. Sci.* **2021**, *22* (1), 181.
(3) Lambrus, B. G.; Cochet-Escartin, O.; Gao, J.; Newmark, P. A.; Collins, E.-M. S.; Collins, J. J. Tryptophan Hydroxylase Is Required for Eye Melanogenesis in the Planarian Schmidtea Mediterranea. *PLoS One* **2015**, *10* (5), No. e0127074.
(4) Vargas, M. A.; Deive, F. J.; Álvarez, M. S.; Longo, M. A.; Rodríguez, A.; Bernal, C.; Martínez, R. Effect of Process Parameters and Surfactant Additives on the Obtained Activity of Recombinant Tryptophan Hydroxylase (TPH1) for Enzymatic Synthesis of 5-Hydroxytryptophan (5-HTP). *Enzyme Microb. Technol.* **2022**, *154*, No. 109975.
(5) Lynn-Bullock, C. P.; Welshhans, K.; Pallas, S. L.; Katz, P. S. The Effect of Oral 5-HTP Administration on 5-HTP and 5-HT Immunoreactivity in Monoaminergic Brain Regions of Rats. *J. Chem. Neuroanat.* **2004**, *27* (2), 129−138.
(6) Agren, H.; Reibring, L.; Hartvig, P.; Tedroff, J.; Bjurling, P.; Hörnfeldt, K.; Andersson, Y.; Lundqvist, H.; Langström, B. Low Brain Uptake of L-[11C]5-Hydroxytryptophan in Major Depression: A Positron Emission Tomography Study on Patients and Healthy Volunteers. *Acta Psychiatr. Scand.* **1991**, *83* (6), 449−455.
(7) Maes, M.; Vandewoude, M.; Schotte, C.; Maes, L.; Martin, M.; Blockx, P. Sex-linked Differences in Cortisol, ACTH and Prolactin Responses to 5-hydroxy-tryptophan in Healthy Controls and Minor and Major Depressed Patients. *Acta Psychiatr. Scand.* **1989**, *80* (6), 584−590.
(8) Fang, X.; Wu, Y.; Dai, Y.; Xiao, H.; Li, S.; Chen, X.; Yuan, M.; Guo, Y.; Ma, L.; Lin, D.; et al. In Situ Recovery of Serotonin Synthesis by a Tryptophan Hydroxylase-Like Nanozyme for the Treatment of Depression. *J. Am. Chem. Soc.* **2025**, *147* (11), 9111−9121.
(9) Weinberg, J.; Lerner, D. A. Theoretical Study of 5-HTP. Potential New Drug Resulting from the Complexation of 5-HTP with ATP. *Comput. Chem.* **2013**, *1* (1), 1−4.
(10) Buckley, N. A.; Dawson, A. H.; Isbister, G. K. Serotonin Syndrome. *BMJ.* **2014**, *348*, No. g1626.
(11) Ross, J. B.; Senear, D. F.; Waxman, E.; Kombo, B. B.; Rusinova, E.; Huang, Y. T.; Laws, W. R.; Hasselbacher, C. A. Spectral Enhancement of Proteins: Biological Incorporation and Fluorescence Characterization of 5-Hydroxytryptophan in Bacteriophage Lambda cI Repressor. *Proc. Natl. Acad. Sci. U. S. A.* **1992**, *89* (24), 12023−12027.
(12) Steward, L. E.; Collins, C. S.; Gilmore, M. A.; Carlson, J. E.; Ross, J. B. A.; Chamberlin, A. R. In Vitro Site-Specific Incorporation of Fluorescent Probes into β-Galactosidase. *J. Am. Chem. Soc.* **1997**, *119* (1), 6−11.
(13) Pastore, A. J.; Ficaretta, E.; Chatterjee, A.; Davidson, V. L. Substitution of the Sole Tryptophan of the Cupredoxin, Amicyanin, with 5-Hydroxytryptophan Alters Fluorescence Properties and Energy Transfer to the Type 1 Copper Site. *J. Inorg. Biochem.* **2022**, *234*, No. 111895.
(14) Mulvaney, S. P.; Keating, C. D. Raman Spectroscopy. *Anal. Chem.* **2000**, *72* (12), 145−158.
(15) Kudelski, A. Analytical Applications of Raman Spectroscopy. *Talanta* **2008**, *76* (1), 1−8.
(16) Jenkins, A. L.; Larsen, R. A.; Williams, T. B. Characterization of Amino Acids Using Raman Spectroscopy. *Spectrochim. Acta. A. Mol. Biomol. Spectrosc.* **2005**, *61* (7), 1585−1594.
(17) Oladepo, S. A.; Xiong, K.; Hong, Z.; Asher, S. A. Elucidating Peptide and Protein Structure and Dynamics: UV Resonance Raman Spectroscopy. *J. Phys. Chem. Lett.* **2011**, *2* (4), 334−344.
(18) Jakubek, R. S.; Handen, J.; White, S. E.; Asher, S. A.; Lednev, I. K. Ultraviolet Resonance Raman Spectroscopic Markers for Protein Structure and Dynamics. *TrAC Trends Anal. Chem.* **2018**, *103*, 223−229.
(19) Sanchez, K. M.; Kang, G.; Wu, B.; Kim, J. E. Tryptophan-Lipid Interactions in Membrane Protein Folding Probed by Ultraviolet Resonance Raman and Fluorescence Spectroscopy. *Biophys. J.* **2011**, *100* (9), 2121−2130.
(20) Milán-Garcés, E. A.; Mondal, S.; Udgaonkar, J. B.; Puranik, M. Intricate Packing in the Hydrophobic Core of Barstar through a CH−π Interaction. *J. Raman Spectrosc.* **2014**, *45* (9), 814−821.
(21) Sanchez, K. M.; Gable, J. E.; Schlamadinger, D. E.; Kim, J. E. Effects of Tryptophan Microenvironment, Soluble Domain, and Vesicle Size on the Thermodynamics of Membrane Protein Folding: Lessons from the Transmembrane Protein OmpA. *Biochemistry* **2008**, *47* (48), 12844−12852.
(22) Sharma, B.; Frontiera, R. R.; Henry, A. I.; Ringe, E.; Van Duyne, R. P. SERS: Materials, Applications, and the Future. *Mater. Today* **2012**, *15* (1−2), 16−25.
(23) dos Santos, D. P.; Temperini, M. L. A.; Brolo, A. G. Single-Molecule Surface-Enhanced (Resonance) Raman Scattering (SE(R)-RS) as a Probe for Metal Colloid Aggregation State. *J. Phys. Chem. C* **2016**, *120* (37), 20877−20885.
(24) dos Santos, D. P.; Temperini, M. L. A.; Brolo, A. G. Intensity Fluctuations in Single-Molecule Surface-Enhanced Raman Scattering. *Acc. Chem. Res.* **2019**, *52* (2), 456−464.
(25) Cardozo, G. C.; Duarte, E. L.; Da Cunha, A. R.; Soga, D.; De Almeida Rizzutto, M.; Lamy, M. T.; Milán-Garcés, E. A. Label-Free Detection of π-Stacking Interactions During Tryptophan Self-Assembling Into Amyloid-Like Structures Using Surface-Enhanced Raman Scattering. *J. Raman Spectrosc.* **2025**, *56* (10), 987−998.
(26) Hernández, B.; Tinacci, L.; Coïc, Y.-M.; Chenal, A.; Cohen, R.; Sanchez-Cortes, S.; Ghomi, M. Tryptophan Tight Binding to Gold Nanoparticles Induces Drastic Changes in Indole Ring Raman Markers. *J. Phys. Chem. C* **2018**, *122* (24), 13034−13046.
(27) Stewart, S.; Fredericks, P. M. Surface-Enhanced Raman Spectroscopy of Amino Acids Adsorbed on an Electrochemically Prepared Silver Surface. *Spectrochim. Acta. A. Mol. Biomol. Spectrosc.* **1999**, *55* (7−8), 1641−1660.
(28) Feliu, N.; Hassan, M.; Garcia Rico, E.; Cui, D.; Parak, W.; Alvarez-Puebla, R. SERS Quantification and Characterization of Proteins and Other Biomolecules. *Langmuir* **2017**, *33* (38), 9711−9730.
(29) Michałowska, A.; Kudelski, A. Applications of Surface Enhanced Raman Scattering (SERS) Spectroscopy for Detection of Nucleic Acids. *Nanophotonics* **2024**, *13* (25), 4577−4603.
(30) Moody, A. S.; Sharma, B. Multi-Metal, Multi-Wavelength Surface-Enhanced Raman Spectroscopy Detection of Neurotransmitters. *ACS Chem. Neurosci.* **2018**, *9* (6), 1380−1387.
(31) Maiti, N.; Thomas, S.; Jacob, J. A.; Chadha, R.; Mukherjee, T.; Kapoor, S. DFT and Surface-Enhanced Raman Scattering Study of Tryptophan−Silver Complex. *J. Colloid Interface Sci.* **2012**, *380* (1), 141−149.
(32) Lee, H. I.; Suh, S. W.; Kim, M. S. Raman Spectroscopy of L-tryptophan-containing Peptides Adsorbed on a Silver Surface. *J. Raman Spectrosc.* **1988**, *19* (7), 491−495.

(33) Takeuchi, H. Raman Structural Markers of Tryptophan and Histidine Side Chains in Proteins. *Biopolymers* **2003**, *72* (5), 305−317.
(34) Song, P.; Guo, X.; Pan, Y.; Wen, Y.; Zhang, Z.; Yang, H. SERS and in Situ SERS Spectroelectrochemical Investigations of Serotonin Monolayers at a Silver Electrode. *J. Electroanal. Chem.* **2013**, *688*, 384−391.
(35) Manciu, F.; Ciubuc, J.; Sundin, E.; Qiu, C.; Bennet, K. Analysis of Serotonin Molecules on Silver Nanocolloids—A Raman Computational and Experimental Study. *Sensors* **2017**, *17* (7), 1471.
(36) Vander Ende, E.; Bourgeois, M. R.; Henry, A. I.; Chávez, J. L.; Krabacher, R.; Schatz, G. C.; Van Duyne, R. P. Physicochemical Trapping of Neurotransmitters in Polymer-Mediated Gold Nanoparticle Aggregates for Surface-Enhanced Raman Spectroscopy. *Anal. Chem.* **2019**, *91* (15), 9554−9562.
(37) Yang, H.; Zhang, X.; Gao, Y.; Peng, Z.; Su, B.; Li, K.; Zhang, C. Detection of Melatonin and 5-HTP in Dietary Supplements Based on Multiple Spectra. *Front. Nutr.* **2025**, *12*, No. 1532092.
(38) Lombardi, J. R.; Birke, R. L. A Unified Approach to Surface-Enhanced Raman Spectroscopy. *J. Phys. Chem. C* **2008**, *112* (14), 5605−5617.
(39) Cong, S.; Liu, X.; Jiang, Y.; Zhang, W.; Zhao, Z. Surface Enhanced Raman Scattering Revealed by Interfacial Charge-Transfer Transitions. *Innovation* **2020**, *1* (3), No. 100051.
(40) Le Ru, E. C.; Auguié, B. Enhancement Factors: A Central Concept during 50 Years of Surface-Enhanced Raman Spectroscopy. *ACS Nano* **2024**, *18* (14), 9773−9783.
(41) Van Der Spoel, D.; Lindahl, E.; Hess, B.; Groenhof, G.; Mark, A. E.; Berendsen, H. J. C. GROMACS: Fast, Flexible, and Free. *J. Comput. Chem.* **2005**, *26* (16), 1701−1718.
(42) Tuckerman, M. E.; Martyna, G. J. Understanding Modern Molecular Dynamics: Techniques and Applications. *J. Phys. Chem. B* **2000**, *104* (2), 159−178.
(43) Orio, M.; Pantazis, D. A.; Neese, F. Density Functional Theory. *Photosynth. Res.* **2009**, *102* (2), 443−453.
(44) Hao, Q.; Chen, Y.; Wei, Y.; Li, G.; Tang, X.; Chen, D.; Zhu, X.; Yao, L.; Zhao, X.; Li, M.; et al. Mechanism Switch in Surface-Enhanced Raman Scattering: The Role of Nanoparticle Dimensions. *J. Phys. Chem. Lett.* **2024**, *15* (28), 7183−7190.
(45) Wu, X.; Cañamares, M. V.; Kakoulli, I.; Sanchez-Cortes, S. Chemical Characterization and Molecular Dynamics Simulations of Bufotenine by Surface-Enhanced Raman Scattering (SERS) and Density Functional Theory (DFT). *J. Phys. Chem. Lett.* **2022**, *13* (25), 5831−5837.
(46) Engberg, O.; Saha Roy, D.; Krupa, P.; Banerjee, S.; Chaudhary, A.; Smith, A. A.; Li, M. S.; Maiti, S.; Huster, D. Molecules in the Serotonin-Melatonin Synthesis Pathway Have Distinct Interactions with Lipid Membranes. *J. Phys. Chem. B* **2025**, *129* (10), 2687−2700.
(47) Lee, P. C.; Meisel, D. Adsorption and Surface-Enhanced Raman of Dyes on Silver and Gold Sols. *J. Phys. Chem.* **1982**, *86* (17), 3391−3395.
(48) Roccatano, D. *A Short Introduction to the Molecular Dynamics Simulation of Nanomaterials*. In Micro and Nanomanufacturing, Vol. II; Jackson, M. J.; Ahmed, W., Eds.; Springer International Publishing: Cham, 2018; pp 123−155.
(49) Brooks, B. R.; Brooks, C. L.; Mackerell, A. D.; Nilsson, L.; Petrella, R. J.; Roux, B.; Won, Y.; Archontis, G.; Bartels, C.; Boresch, S.; et al. CHARMM: The Biomolecular Simulation Program. *J. Comput. Chem.* **2009**, *30* (10), 1545−1614.
(50) Gfeller, D.; Michielin, O.; Zoete, V. SwissSidechain: A Molecular and Structural Database of Non-Natural Sidechains. *Nucleic Acids Res.* **2012**, *41* (D1), D327−D332.
(51) Jorgensen, W. L.; Chandrasekhar, J.; Madura, J. D.; Impey, R. W.; Klein, M. L. Comparison of Simple Potential Functions for Simulating Liquid Water. *J. Chem. Phys.* **1983**, *79* (2), 926−935.
(52) Berendsen, H. J. C.; Postma, J. P. M.; Van Gunsteren, W. F.; DiNola, A.; Haak, J. R. Molecular Dynamics with Coupling to an External Bath. *J. Chem. Phys.* **1984**, *81* (8), 3684−3690.
(53) Evans, D. J.; Holian, B. L. The Nose−Hoover Thermostat. *J. Chem. Phys.* **1985**, *83* (8), 4069−4074.
(54) Parrinello, M.; Rahman, A. Polymorphic Transitions in Single Crystals: A New Molecular Dynamics Method. *J. Appl. Phys.* **1981**, *52* (12), 7182−7190.
(55) Essmann, U.; Perera, L.; Berkowitz, M. L.; Darden, T.; Lee, H.; Pedersen, L. G. A Smooth Particle Mesh Ewald Method. *J. Chem. Phys.* **1995**, *103* (19), 8577−8593.
(56) Hess, B.; Bekker, H.; Berendsen, H. J. C.; Fraaije, J. G. E. M. LINCS: A Linear Constraint Solver for Molecular Simulations. *J. Comput. Chem.* **1997**, *18* (12), 1463−1472.
(57) Muniz-Miranda, M.; Pergolese, B.; Bigotto, A. SERS and DFT Investigation on the Adsorption of 1,10-Phenanthroline on Transition Metal Surfaces. *Phys. Chem. Chem. Phys.* **2010**, *12* (5), 1145−1151.
(58) Aliaga, A. E.; Osorio-Román, I.; Leyton, P.; Garrido, C.; Cárcamo, J.; Caniulef, C.; Célis, F.; Díaz Fleming, G.; Clavijo, E.; Gómez-Jeria, J. S.; Campos-Vallette, M. M. Surface-Enhanced Raman Scattering Study of L-Tryptophan. *J. Raman Spectrosc.* **2009**, *40* (2), 164−169.
(59) The PyMOL Molecular Graphics System, Version 3.0 Schrödinger, LLC. https://www.pymol.org.
(60) Frisch, M. J.; Trucks, G. W.; Schlegel, H. B.; Scuseria, G. E.; Robb, M. A.; Cheeseman, J. R.; Scalmani, G.; Barone, V.; Mennucci, B.; Petersson, G. A.; et al.*Gaussian 09, Revision E.01*; Gaussian, Inc.: Wallingford CT, 2009.
(61) Zhao, Y.; Truhlar, D. G. Applications and Validations of the Minnesota Density Functionals. *Chem. Phys. Lett.* **2011**, *502* (1−3), 1−13.
(62) Chiodo, S.; Russo, N.; Sicilia, E. LANL2DZ Basis Sets Recontracted in the Framework of Density Functional Theory. *J. Chem. Phys.* **2006**, *125* (10), 104107.
(63) Legge, F. S.; Nyberg, G. L.; Peel, J. B. DFT Calculations for Cu-, Ag-, and Au-Containing Molecules. *J. Phys. Chem. A* **2001**, *105* (33), 7905−7916.
(64) Mennucci, B. Polarizable Continuum Model. *WIREs Comput. Mol. Sci.* **2012**, *2* (3), 386−404.
(65) Jamróz, M. H. *Vibrational Energy Distribution Analysis VEDA 4, Warsaw*, 2004−2010.
(66) Chemcraft—Graphical Software for Visualization of Quantum Chemistry Computations. Version 1.8, Build 682. https://www.chemcraftprog.com.
(67) Londoño-Lemos, M. E.; Martínez-Bulit, P.; López-Sandoval, H.; Gracia-Mora, I.; Sánchez-Bartez, F.; Castro-Jiménez, T.; Duarte-Hernández, A. M.; Flores-Parra, A.; Contreras, R.; Barba-Behrens, N. Transition Metal Coordination Compounds of an Antiobesity Serotoninergic Ligand: Spectroscopic Characterization and Adipogenesis Activity. *Transit. Met. Chem.* **2017**, *42* (7), 587−596.
(68) Wakahara, A.; Kido, M.; Fujiwara, T.; Tomita, K. Structural Studies of Tryptophan Metabolites by X-Ray Diffraction Method. I. The Crystal and Molecular Structure of 5-Hydroxy-DL-Tryptophan. *Bull. Chem. Soc. Jpn.* **1973**, *46* (8), 2475−2480.
(69) Laury, M. L.; Carlson, M. J.; Wilson, A. K. Vibrational Frequency Scale Factors for Density Functional Theory and the Polarization Consistent Basis Sets. *J. Comput. Chem.* **2012**, *33* (30), 2380−2387.
(70) Miura, T.; Takeuchi, H.; Harada, I. Tryptophan Raman Bands Sensitive to Hydrogen Bonding and Side-chain Conformation. *J. Raman Spectrosc.* **1989**, *20* (10), 667−671.
(71) Chuang, C.-H.; Chen, Y.-T. Raman Scattering of L-Tryptophan Enhanced by Surface Plasmon of Silver Nanoparticles: Vibrational Assignment and Structural Determination. *J. Raman Spectrosc.* **2009**, *40* (2), 150−156.
(72) Kim, S. K.; Kim, M. S.; Suh, S. W. Surface-enhanced Raman Scattering (SERS) of Aromatic Amino Acids and Their Glycyl Dipeptides in Silver Sol. *J. Raman Spectrosc.* **1987**, *18* (3), 171−175.
(73) Hernández, B.; Pflüger, F.; Adenier, A.; Kruglik, S. G.; Ghomi, M. Vibrational Analysis of Amino Acids and Short Peptides in Hydrated Media. VIII. Amino Acids with Aromatic Side Chains: L-

Phenylalanine, l-Tyrosine, and l-Tryptophan. *J. Phys. Chem. B* **2010**, *114* (46), 15319−15330.
(74) Marin, J. H.; Temperini, M. L. A.; Ando, R. A. SERS and Resonance Raman of 5-Nitroisatin on Silver − The Distinction between the Coordination and Surface Complexes. *Spectrochim. Acta. A. Mol. Biomol. Spectrosc.* **2021**, *263*, No. 120163.
(75) Mdluli, P. S.; Sosibo, N. M.; Mashazi, P. N.; Nyokong, T.; Tshikhudo, R. T.; Skepu, A.; Van der Lingen, E. Selective Adsorption of PVP on the Surface of Silver Nanoparticles: A Molecular Dynamics Study. *J. Mol. Struct.* **2011**, *1004* (1−3), 131−137.
(76) Pagliai, M.; Bellucci, L.; Muniz-Miranda, M.; Cardini, G.; Schettino, V. A Combined Raman, DFT and MD Study of the Solvation Dynamics and the Adsorption Process of Pyridine in Silver Hydrosols. *Phys. Chem. Chem. Phys.* **2006**, *8* (1), 171−178.
(77) Eom, S. Y.; Lee, Y. R.; Kwon, C. H.; Kim, H. L. Surface Enhanced Raman Scattering of 2,2′-Biphenyl Dicarboxylic Acid on Silver Surfaces: Structure and Orientation upon Adsorption. *J. Mol. Struct.* **2016**, *1115*, 70−74.

https://doi.org/10.1021/acs.jpcc.5c06154
J. Phys. Chem. C 2025, 129, 20313−20326